Control of the Vertical Gradient Freeze crystal growth process via backstepping

Stefan Ecklebe * **Frank Woittennek** ** **Jan Winkler** *

* *Institute of Control Theory, Technische Universität Dresden, 01069 Dresden, Germany (email: {stefan.ecklebe, jan.winkler}@tu-dresden.de)*
** *Institute of Automation and Control Engineering, University of Health Sciences, Medical Informatics and Technology, 6060 Hall in Tirol, Austria (email: frank.woittennek@umit.at)*

Abstract: This contribution presents a backstepping-based state feedback design for the tracking control of a two-phase Stefan problem which is encountered in the Vertical Gradient Freeze crystal growth process. A two-phase Stefan problem consists of two coupled free boundary problems and is a vital part of many crystal growth processes due to the time-varying extent of crystal and melt during growth. In addition, a different approach for the numerical approximation of the backstepping transformations kernel is presented.

Keywords: Vertical Gradient Freeze, two-phase Stefan problem, distributed-parameter systems, backstepping, tracking control, numerical methods

1. INTRODUCTION

The Vertical Gradient Freeze (VGF) crystal growth process is used for the production of high efficiency bulk compound semiconductor single crystals like Gallium-Arsenide (GaAs) or Indium-Phosphide (Jurisch et al., 2005). The process basically works as follows: A seed crystal is placed at the bottom of a rotationally symmetric crucible which is later filled with solid semiconductor chunks. After all material (up to the seed) in the crucible is molten, a vertical temperature gradient is moved through the plant such that a single crystal grows from the bottom to the top in a desired manner. This is done by manipulating the power of the heaters which surround the crucible. Modelling of the system yields two coupled free boundary problems (FBPs) for crystal and melt that form the so called two-phase Stefan problem (TPSP) e.g. (Crank, 1984) which is inherently nonlinear.

Due to the spatial extent of the system it is broadly discussed in the framework of distributed parameter systems. Making the assumption that the temperature distribution in one phase is constant (which is often justified due to its dominant spatial extent) yields the so called one-phase Stefan problem (OPSP). Regarding this special case, results are lately available for the feedforward design by Dunbar et al. (2003), as well as for feedback designs using enthalpy- (Petrus et al., 2012, 2014), geometry- (Maidi and Corriou, 2016) or backstepping- (Koga et al., 2019) based approaches. Regarding the full problem, (Rudolph et al., 2003, 2004) extend the flatness-based motion planning to the two-phase case, while (Kang and Zabaras, 1995) and (Hinze et al., 2009) address the problem from the side of optimal control. Concerning feedback, a direct extension of the approaches for the one-phase variant is not feasible since the coupling between the two FBPs has to be taken into account here. In this context it is noteworthy that (Petrus et al., 2010) already states a Lyapunov-based control law for the TPSP with actuation at one boundary and that (Koga and Krstic, 2019) does the same via an energy-shaping approach. However, a gap to the tracking control of the complete TPSP using both inputs remained. In (Ecklebe et al., 2019) the authors present different output feedback designs using energy- and flatness-based approaches, rendering backstepping-based designs the last remaining problem.

1.1 Objective and Structure

The main objective of this contribution is to present a tracking control for the TPSP by backstepping-based state feedback. Furthermore, a different approach for the numeric approximation of the resulting time-variant backstepping kernels is presented. Due to the limited space, this is done in a rather brief fashion and more detailed results will be given in a forthcoming publication.

In Section 2 a simplified one-dimensional distributed parameter model of the process is introduced, before Section 3 briefly recites the feedforward control design and states some properties of the derived trajectories which are required for the tracking control later on. Based on these, Section 4 derives a suitable error system as well as the corresponding target dynamics for it and states the resulting tracking control law. In Section 5, the existence of solutions for the kernel equations as well as a new computation scheme to solve them is discussed, before Section 6 briefly presents simulation results. Finally, a summary and an outlook to further work is given.

⋆ This work has been funded by the Deutsche Forschungsgemeinschaft (DFG) [project number WI 4412/1-1].

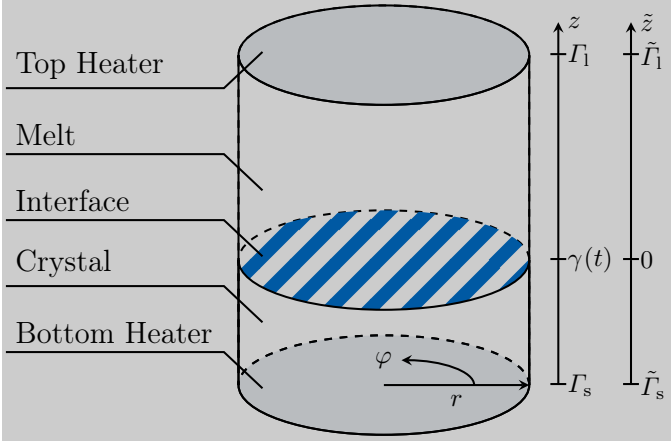

Fig. 1. Schematics of the cylindrical coordinates (r, φ, z) and the moving coordinate frame $\tilde{z} = z - \gamma(t)$.

2. MODELLING

As the foundation for model based control, this section introduces a one dimensional distributed parameter model of the VGF process plant.

2.1 Plant Model

The quantity under consideration is given by the spatial and temporal distribution of the system temperature T in the crucible, denoted in cylindrical coordinates with radius r, angle φ as well as height z, and depending on the time t. Within this contribution, we assume that the lateral heaters are used as active isolation, avoiding any heat loss in radial direction and therefore yielding a temperature distribution which is independent of r. Since the plant is also rotationally symmetric, this justifies averaging over the longitudinal cross-sectional area, reducing the spatial domain to a line whose boundaries are represented by the bottom and top of the crucible at $z = \Gamma_\mathrm{s}$ and $z = \Gamma_\mathrm{l}$, respectively. This yields two areas given by the crystal and the melt, separated by the moving phase boundary $\gamma(t)$ (cf. Figure 1). In contrast to the temperature distribution in the crystal, which can be modelled via diffusion, the liquid melt also enables convective heat transport. However, since the considered semi-conductors posses small Prandtl numbers (e.g. 0.068 for GaAs), the dominating heat transport mechanism is diffusion. Therefore, convective effects in the melt are neglected.

Summarising, the temperature distribution in the system is given by the distributed variable $T(z,t)$ and governed by a one dimensional nonlinear heat equation (Cannon, 1984)

$$\frac{\partial}{\partial t}\Big(\rho(T(z,t))c_\mathrm{p}(T(z,t))T(z,t)\Big) = \frac{\partial}{\partial z}\left(\lambda(T(z,t))\frac{\partial}{\partial z}T(z,t)\right), z \in (\Gamma_\mathrm{s}, \Gamma_\mathrm{l}) \setminus \{\gamma(t)\} \quad (1)$$

with the density ρ, the specific heat capacity c_p, and λ the thermal conductivity being temperature-dependent. Note, that while the temperature at the interface $T(\gamma(t),t)$ is fixed at the melting point temperature T_m due to the ongoing phase transition, the heat flow in this description is not continuous at the phase boundary due to the release of latent heat within the solidification process and the abrupt change of the physical parameters between crystal and melt.

2.2 Decomposition

Assuming piecewise constant parameters for the solid and the liquid phase it is possible to decompose the tempearature distribution via

$$T(z,t) = \begin{cases} T_\mathrm{s}(z,t), & z \in \Omega_\mathrm{s} = (\Gamma_\mathrm{s}, \gamma(t)) \\ T_\mathrm{l}(z,t), & z \in \Omega_\mathrm{l} = (\gamma(t), \Gamma_\mathrm{l}) \end{cases} \quad (2)$$

with the temperatures $T_\mathrm{s}(z,t)$ and $T_\mathrm{l}(z,t)$ in the solid and liquid part, respectively. This yields the two FBPs

$$\partial_t T_\mathrm{s}(z,t) = \alpha_\mathrm{s}\partial_z^2 T_\mathrm{s}(z,t) \quad (3a)$$
$$\partial_z T_\mathrm{s}(\Gamma_\mathrm{s},t) = \frac{\delta_\mathrm{s}}{\lambda_\mathrm{s}} u_\mathrm{s}(t) \quad (3b)$$
$$T_\mathrm{s}(\gamma(t),t) = T_\mathrm{m} \quad (3c)$$
$$\partial_t T_\mathrm{l}(z,t) = \alpha_\mathrm{l}\partial_z^2 T_\mathrm{l}(z,t) \quad (3d)$$
$$\partial_z T_\mathrm{l}(\Gamma_\mathrm{l},t) = \frac{\delta_\mathrm{l}}{\lambda_\mathrm{l}} u_\mathrm{l}(t) \quad (3e)$$
$$T_\mathrm{l}(\gamma(t),t) = T_\mathrm{m} \quad (3f)$$

where the indexes "s" and "l" denote the solid and liquid phase, respectively. Furthermore, the heat flows $u_\mathrm{s}(t)$ and $u_\mathrm{l}(t)$ at the bottom and the top boundary are considered as system inputs with the orientation factors $\delta_\mathrm{s} = -1$ and $\delta_\mathrm{l} = 1$. For reasons of clarity, the partial derivative of $T(z,t)$ wrt. z and t are given by $\partial_z T(z,t)$ and $\partial_t T(z,t)$, respectively. Finally, $\alpha_\mathrm{s} = \lambda_\mathrm{s}/(\rho_\mathrm{s} c_\mathrm{p,s})$ and $\alpha_\mathrm{l} = \lambda_\mathrm{l}/(\rho_\mathrm{l} c_\mathrm{p,l})$ denote the thermal diffusivities.

Next, examining the energy balance at the interface $\gamma(t)$ yields the Stefan condition (Stefan, 1891)

$$\rho_\mathrm{m} L\dot{\gamma}(t) = \lambda_\mathrm{s}\partial_z T_\mathrm{s}(\gamma(t),t) - \lambda_\mathrm{l}\partial_z T_\mathrm{l}(\gamma(t),t) \quad (4)$$

which describes the evolution of the phase boundary. Herein, ρ_m denotes the density of the melt at melting temperature and L the specific latent heat.

Together, (3) and (4) form the TPSP whose state is given by

$$\boldsymbol{x}(\cdot,t) = \begin{pmatrix} T(\cdot,t) \\ \gamma(t) \end{pmatrix} \in X = L_2([\Gamma_\mathrm{s}, \Gamma_\mathrm{l}]) \times (\Gamma_\mathrm{s}, \Gamma_\mathrm{l}), \quad (5)$$

where $L_2([\Gamma_\mathrm{s}, \Gamma_\mathrm{l}])$ denotes the space of real-valued square-integrable functions defined on $[\Gamma_\mathrm{s}, \Gamma_\mathrm{l}]$. Note that the PDE-ODE-PDE system defined by (3) and (4) is inherently nonlinear since the domains of (3a) and (3d) depend on the state variable $\gamma(t)$.

Since the systems (3a)–(3c) and (3d)–(3f) share the same structure, the following sections will merely discuss generic variables, denoted by the $\circ$ symbol if the results are applicable to both phases. If terms from two different phases are to appear in the same expression, the complementary phase is marked by the $\bullet$ symbol.

2.3 Moving Coordinates

To simplify the notation of the controller error system later on, the coordinate transformation

$$\tilde{T}(\tilde{z},t) = T(z,t) \quad \text{with} \quad \tilde{z} \coloneqq z - \gamma(t) \quad (6)$$

is introduced which maps the current interface position to the origin of a moving frame as shown in Figure 1. This yields the generic system in the new coordinates

$$\partial_t \tilde{T}_\circ(\tilde{z},t) = \alpha_\circ \partial_{\tilde{z}}^2 \tilde{T}_\circ(\tilde{z},t) + \dot{\gamma}(t)\partial_{\tilde{z}}\tilde{T}_\circ(\tilde{z},t) \tag{7a}$$

$$\partial_{\tilde{z}}\tilde{T}_\circ(\tilde{\Gamma}_\circ,t) = \frac{\delta_\circ}{\lambda_\circ}u_\circ(t) \tag{7b}$$

$$\tilde{T}_\circ(0,t) = T_\mathrm{m} \tag{7c}$$

$$\dot{\gamma}(t) = s_\circ \partial_{\tilde{z}}\tilde{T}_\circ(0,t) + s_\bullet \partial_{\tilde{z}}\tilde{T}_\bullet(0,t) \tag{7d}$$

where $\tilde{\Gamma}_\circ = \Gamma_\circ - \gamma(t)$, $s_\circ = -\delta_\circ\lambda_\circ/(L\rho_\mathrm{m})$, and $s_\bullet = -\delta_\bullet\lambda_\bullet/(L\rho_\mathrm{m})$. Note, that in these coordinates the interface velocity $\dot{\gamma}(t)$ directly enters the PDE (7a) in form of a convection coefficient.

3. FEEDFORWARD CONTROL

This section outlines a feedforward control that originates from Dunbar et al. (2003) for the OPSP and was extended by Rudolph et al. (2003) to the TPSP. Since the trajectories for $T(z,t)$ and $\gamma(t)$, which are computed by this feedforward scheme, will be used as a reference in following sections, this recap is merely focussed on their properties.

Since the solution $\tilde{T}_\circ(\tilde{z},t)$ of (7) can be expressed in terms of an infinite power series in $\tilde{z}$, given by

$$\tilde{T}_\circ(\tilde{z},t) = \sum_{i=0}^{\infty} c_{\circ,i}(t)\frac{\tilde{z}^i}{i!}\,, \tag{8}$$

substitution into (7a) and comparison of the coefficients of like powers in $\tilde{z}$ yields the recursion formula

$$c_{\circ,i+2}(t) = \frac{1}{\alpha_\circ}\big(\partial_t c_{\circ,i}(t) - \dot{\gamma}(t)c_{\circ,i+1}(t)\big)\ i = 0,\dots,\infty\,. \tag{9}$$

Examining (8) indicates that the initial coefficients of the series are given by

$$c_{\circ,0}(t) = \tilde{T}_\circ(0,t) = T_\mathrm{m}, \quad c_{\circ,1}(t) = \partial_{\tilde{z}}\tilde{T}_\circ(0,t)\,. \tag{10}$$

Next, using (7d) as the defining equation for the melt-gradient

$$\partial_{\tilde{z}}\tilde{T}_\mathrm{l}(0,t) = \frac{1}{\lambda_\mathrm{l}}\left(\lambda_\mathrm{s}\partial_{\tilde{z}}\tilde{T}_\mathrm{s}(0,t) - \rho_\mathrm{m}L\dot{\gamma}(t)\right)\,, \tag{11}$$

the solution for both phases can be expressed by the gradient in the crystal $\partial_{\tilde{z}}\tilde{T}_\mathrm{s}(0,t)$ and the growth rate $\dot{\gamma}(t)$. Thus, (7) via the parametrisation (8) is differentially flat with a flat output

$$\boldsymbol{y}(t) = \begin{pmatrix} y_1(t) \\ y_2(t) \end{pmatrix} = \begin{pmatrix} \partial_{\tilde{z}}\tilde{T}_\mathrm{s}(0,t) \\ \gamma(t) \end{pmatrix}. \tag{12}$$

Furthermore, reference trajectories for the components $y_{\mathrm{r},i}(t)$ of $\boldsymbol{y}_\mathrm{r}(t)$ are chosen as transitions between stationary states $y_{\mathrm{r},i}^0$ and $y_{\mathrm{r},i}^\mathrm{e}$ for start and end, respectively, via

$$y_{\mathrm{r},i}(t) = y_{\mathrm{r},i}^0 + (y_{\mathrm{r},i}^\mathrm{e} - y_{\mathrm{r},i}^0)\Phi(t) \quad i = 1,2 \tag{13}$$

with $\Phi(t)$ sufficiently smooth.

Analysing the specific convergence conditions for (8), (Rudolph et al., 2003, 2004) show that it is sufficient to demand $\Phi(t) \in \mathcal{G}_{\aleph\leq 2}(\mathbb{R}^+)$ with the Gevrey class $\mathcal{G}_\aleph(\Omega)$ from the definition below.

Definition 1. (Gevrey-class; Gevrey 1918). A smooth function $t \mapsto f(t)$ defined on the open set $\Omega \subset \mathbb{R}$ is an element of the Gevrey class $\mathcal{G}_\aleph(\Omega)$ of order $\aleph$ over Ω if there exists a positive constant D such that

$$\sup_{t\in\Omega}|\partial_t^n f(t)| \leq D^{n+1}\,(n!)^\aleph$$

holds for all n in $\mathbb{N}_0$.

Thus, given the definition of the flat output (12) the reference interface trajectory $\gamma_\mathrm{r}(t)$ is from $\mathcal{G}_{\aleph\leq 2}(\mathbb{R}^+)$. Moreover, as the reference temperature distribution $\tilde{T}_\mathrm{r}(\tilde{z},t)$ is computed via (9) and (8), by construction $\tilde{T}_\mathrm{r}(\tilde{z},t)$ belongs to $\mathcal{K}_{\aleph\leq 2}(\tilde{\Omega},\mathbb{R}^+)$ as defined below.

Definition 2. (Class $\mathcal{K}_\aleph(\Omega_z,\Omega_t)$). A function $(z,t)\mapsto f(z,t)$ is an element of the function class $\mathcal{K}_\aleph(\Omega_z,\Omega_t)$ if $f(\cdot,t)\in\mathcal{C}^\infty(\Omega_z)$ and $f(z,\cdot)\in\mathcal{G}_\aleph(\Omega_t)$.

4. STATE FEEDBACK

The following section states the main result of this contribution concerning the backstepping-based state feedback.

4.1 Error System

For the system (7), let the error coordinates be given by

$$\tilde{e}_\circ(\tilde{z},t) = \tilde{T}_\circ(\tilde{z},t) - \tilde{T}_{\circ,\mathrm{r}}(\tilde{z},t) \tag{14a}$$

$$\Delta\gamma(t) = \gamma(t) - \gamma_\mathrm{r}(t), \tag{14b}$$

yielding the nonlinear error dynamics

$$\begin{aligned}\partial_t\tilde{e}_\circ(\tilde{z},t) = \alpha_\circ\partial_{\tilde{z}}^2\tilde{e}_\circ(\tilde{z},t) + \big(\Delta\dot{\gamma}(t)\partial_{\tilde{z}} + \dot{\gamma}_\mathrm{r}(t)\partial_{\tilde{z}}\big)\tilde{e}_\circ(\tilde{z},t)\\ + \Delta\dot{\gamma}(t)\partial_{\tilde{z}}\tilde{T}_{\circ,\mathrm{r}}(\tilde{z},t)\end{aligned} \tag{15}$$

as shown in Appendix A. Linearising (15) around the reference ($e_\circ(\tilde{z},t)\equiv 0, \Delta\gamma(t) = 0$) yields the linearised error dynamics

$$\begin{aligned}\partial_t\tilde{e}_\circ(\tilde{z},t) = \alpha_\circ\partial_{\tilde{z}}^2\tilde{e}_\circ(\tilde{z},t) + \dot{\gamma}_\mathrm{r}(t)\partial_{\tilde{z}}\tilde{e}_\circ(\tilde{z},t)\\ + \Delta\dot{\gamma}(t)\partial_{\tilde{z}}\tilde{T}_{\circ,\mathrm{r}}(\tilde{z},t)\end{aligned} \tag{16}$$

as well as

$$\Delta\dot{\gamma}(t) = s_\circ\partial_{\tilde{z}}\tilde{e}_\circ(0,t) + s_\bullet\partial_{\tilde{z}}\tilde{e}_\bullet(0,t). \tag{17}$$

Hence, substituting (17) in (16) gives the linear time-variant error system

$$\begin{aligned}\partial_t\tilde{e}_\circ(\tilde{z},t) = \alpha_\circ\partial_{\tilde{z}}^2\tilde{e}_\circ(\tilde{z},t) + \dot{\gamma}_\mathrm{r}(t)\partial_{\tilde{z}}\tilde{e}_\circ(\tilde{z},t)\\ + b_\circ(\tilde{z},t)\partial_{\tilde{z}}\tilde{e}_\circ(0,t) + c_\circ(\tilde{z},t)\partial_{\tilde{z}}\tilde{e}_\bullet(0,t)\end{aligned} \tag{18a}$$

$$\partial_{\tilde{z}}\tilde{e}_\circ(\tilde{\Gamma}_\circ,t) = \tilde{u}_\circ(t) \tag{18b}$$

$$\tilde{e}_\circ(0,t) = 0 \tag{18c}$$

$$\Delta\dot{\gamma}(t) = s_\circ\partial_{\tilde{z}}\tilde{e}_\circ(0,t) + s_\bullet\partial_{\tilde{z}}\tilde{e}_\bullet(0,t) \tag{18d}$$

with $b_\circ(\tilde{z},t) = s_\circ\partial_{\tilde{z}}\tilde{T}_{\circ,\mathrm{r}}(\tilde{z},t)$, $c_\circ(\tilde{z},t) = s_\bullet\partial_{\tilde{z}}\tilde{T}_{\circ,\mathrm{r}}(\tilde{z},t)$, and the new input $\tilde{u}_\circ(t)$. Note that herein, the solid and liquid temperature errors are coupled over the whole domain by means of their fluxes through the phase boundary.

4.2 Hopf-Cole Transformation

Since the coefficient $\dot{\gamma}_\mathrm{r}(t)$ of the convection term cannot be treated via the classic backstepping transform, it is eliminated by a Hopf-Cole transformation (Hopf, 1950)

$$\tilde{e}_\circ(\tilde{z},t) = \Psi_\circ(\tilde{z},t)\,\bar{e}_\circ(\tilde{z},t) \tag{19}$$

and choosing $\Psi_\circ(\tilde{z},t) = \exp\left(-\frac{\dot{\gamma}_\mathrm{r}(t)}{2\alpha_\circ}\tilde{z}\right)$, which is a standard procedure in these cases. This yields the system

$$\begin{aligned}\partial_t\bar{e}_\circ(\tilde{z},t) = \alpha_\circ\partial_{\tilde{z}}^2\bar{e}_\circ(\tilde{z},t) + r_\circ(\tilde{z},t)\bar{e}_\circ(\tilde{z},t)\\ + \bar{b}_\circ(\tilde{z},t)\partial_{\tilde{z}}\bar{e}_\circ(0,t) + \bar{c}_\circ(\tilde{z},t)\partial_{\tilde{z}}\bar{e}_\bullet(0,t)\end{aligned} \tag{20a}$$

$$\partial_{\tilde{z}}\bar{e}_\circ(\tilde{\Gamma}_\circ,t) = \frac{\dot{\gamma}_\mathrm{r}(t)}{2\alpha_\circ}\bar{e}_\circ(\tilde{\Gamma}_\circ,t) + \Psi_\circ^{-1}(\tilde{\Gamma}_\circ,t)\tilde{u}_\circ(t) \tag{20b}$$

$$\bar{e}_\circ(0,t) = 0 \tag{20c}$$

$$\Delta\dot{\gamma}(t) = s_\circ\partial_{\tilde{z}}\bar{e}_\circ(0,t) + s_\bullet\partial_{\tilde{z}}\bar{e}_\bullet(0,t) \tag{20d}$$

where

$$r_0(\tilde{z},t) = -\frac{1}{4\alpha_\circ}\left(2\ddot{\gamma}_\mathrm{r}(t)\tilde{z} + \dot{\gamma}_\mathrm{r}^2(t)\right) \tag{21a}$$

$$\bar{b}_\circ(\tilde{z},t) = \Psi_\circ^{-1}(\tilde{z},t)\, b_\circ(\tilde{z},t) \tag{21b}$$

$$\bar{c}_\circ(\tilde{z},t) = \Psi_\bullet^{-1}(\tilde{z},t)\, c_\circ(\tilde{z},t). \tag{21c}$$

Note, that the resulting system now exhibits reactive terms that are driven by the reference interface velocity and acceleration. Furthermore, the original Neumann boundary condition now appears as a Robin boundary condition.

4.3 Backstepping Transformation

To enforce proper tracking of the reference, the errors in temperature and boundary position should converge to zero. This demand is formulated in the target system

$$\partial_t w_\circ(\tilde{z},t) = \alpha_\circ \partial_{\tilde{z}}^2 w_\circ(\tilde{z},t) + \mu_\circ(\tilde{z},t) w_\circ(\tilde{z},t) \tag{22a}$$

$$\partial_{\tilde{z}} w_\circ(\tilde{\Gamma}_\circ,t) = \delta_\circ \nu_\circ w_\circ(\tilde{\Gamma}_\circ,t) \tag{22b}$$

$$w_\circ(0,t) = 0 \tag{22c}$$

with the reaction coefficient $\mu_\circ(\tilde{z},t)$ and boundary gain $\nu_\circ$ as design parameters. To map the system (20) into (22) the transformation

$$w_\circ(\tilde{z},t) = \bar{e}_\circ(\tilde{z},t) - \int_0^{\tilde{z}} \tilde{k}_\circ(\tilde{z},\zeta,t)\bar{e}_\circ(\zeta,t)\,\mathrm{d}\zeta \tag{23}$$

is used. Computing the requirements on the transformation kernel $\tilde{k}_\circ(\tilde{z},\zeta,t)$ (cf. Appendix B) yields the kernel equations

$$\begin{aligned}\partial_t \tilde{k}_\circ(\tilde{z},\zeta,t) = \alpha_\circ &\left(\partial_{\tilde{z}}^2 \tilde{k}_\circ(\tilde{z},\zeta,t) - \partial_\zeta^2 \tilde{k}_\circ(\tilde{z},\zeta,t)\right) \\ &+ a_\circ(\zeta,t)\tilde{k}_\circ(\tilde{z},\zeta,t)\end{aligned} \tag{24a}$$

$$2\alpha_\circ \tilde{k}_\circ(\tilde{z},\tilde{z},t) = \int_0^{\tilde{z}} a_\circ(\zeta,t)\,\mathrm{d}\zeta - 2\bar{b}_\circ(\tilde{z},t) \tag{24b}$$

$$\alpha_\circ \tilde{k}_\circ(\tilde{z},0,t) = \int_0^{\tilde{z}} \bar{b}_\circ(\zeta,t)\tilde{k}_\circ(\tilde{z},\zeta,t)\,\mathrm{d}\zeta - \bar{b}_\circ(\tilde{z},t) \tag{24c}$$

$$0 = \int_0^{\tilde{z}} \bar{c}_\circ(\zeta,t)\tilde{k}_\circ(\tilde{z},\zeta,t)\,\mathrm{d}\zeta - \bar{c}_\circ(\tilde{z},t) \tag{24d}$$

where $a_\circ(\tilde{z},t) = \mu_\circ(\tilde{z},t) - r_\circ(\tilde{z},t)$. Examining the system (24), one observes that the problem for $\tilde{k}_\circ(\tilde{z},\zeta,t)$, given by (24a)–(24c) is well-posed (cf. 5.2). Herein, the integral boundary condition (24c) arises since the term $\bar{b}_\circ(\tilde{z},t)\partial_{\tilde{z}}\bar{e}_\circ(0,t)$ is to be eliminated from (20a). However, the demand for completely decoupled target systems and, thus, the elimination of $\bar{c}_\circ(\tilde{z},t)\partial_{\tilde{z}}\bar{e}_\bullet(0,t)$ that results in (24d) renders the problem overdetermined. Therefore, to recover a well-posed formulation the convective coupling at $\tilde{z}=0$ is reintroduced with the modified target system dynamics

$$\begin{aligned}\partial_t \bar{w}_\circ(\tilde{z},t) = \alpha_\circ &\partial_{\tilde{z}}^2 \bar{w}_\circ(\tilde{z},t) \\ &+ \mu_\circ(\tilde{z},t)\bar{w}_\circ(\tilde{z},t) + d_\circ(\tilde{z},t)\partial_{\tilde{z}}\bar{w}_\bullet(0,t)\end{aligned} \tag{25}$$

where $d_\circ(\tilde{z},t) = \int^{\tilde{z}} \bar{c}_\circ(\zeta,t)\tilde{k}_\circ(\tilde{z},\zeta,t)\,\mathrm{d}\zeta - \bar{c}_\circ(\tilde{z},t)$ replaces (24d). Obviously, by choosing $\mu_\circ(\tilde{z},t) \leq 0\ \forall(\tilde{z},t)$ and $\nu \leq 0$ this approach yields exponentially stable error dynamics for the one-phase case where the gradient in the adjacent phase vanishes from (17). For the two-phase case, stability of the resulting error dynamics has to be shown due to the bilateral coupling via $d_\circ(\tilde{z},t)$. This will be addressed in a forthcoming publication due to lack of space. However, simulation studies yield promising results as Section 6 shows. Certainly, for both variants the target systems properties can only be conveyed if the inverse transformation of (23) exists. This can be assumed since it is of Volterra-type and therefore always invertible (cf. Heuser 1992) or shown by a simple fixed-point argument [1].

Finally, by examining (22b), eliminating the target terms via (23) and substituting (20b), the control input for the original system with the kernel in original coordinates $k_\circ(z,\zeta,t) = \tilde{k}_\circ(\tilde{z},\zeta,t)$ is given by

$$\begin{aligned}u_\circ(t) = \frac{\lambda_\circ}{\delta_\circ}\Bigg[&\left(k_\circ(\Gamma_\circ,\Gamma_\circ,t) + \delta_\circ\nu_\circ - \frac{\dot{\gamma}_\mathrm{r}(t)}{2\alpha_\circ}\right)\times \\ &\left(T_\circ(\Gamma_\circ,t) - T_{\circ,\mathrm{r}}(\Gamma_\circ,t)\right) + \partial_z T_{\circ,\mathrm{r}}(\Gamma_\circ,t) \\ &+ \int_{\gamma(t)}^{\Gamma_\circ}\left(\partial_z k_\circ(\Gamma_\circ,\zeta,t) + \delta_\circ\nu k_\circ(\Gamma_\circ,\zeta,t)\right)\times \\ &\left(T(\zeta,t) - T_{\circ,\mathrm{r}}(\zeta,t)\right)\exp\left(\frac{\dot{\gamma}_\mathrm{r}(t)}{2\alpha_\circ}(\zeta-\Gamma_\circ)\right)\mathrm{d}\zeta\Bigg].\end{aligned} \tag{26}$$

5. WELL-POSEDNESS AND NUMERICAL SOLUTION OF THE KERNEL EQUATIONS

In this section, a numerical solution scheme for the kernel equations (24a)–(24c) is discussed [2]. To this end, the integral form of the system is derived in a first step. As stated in (Jadachowski et al., 2012), the method of successive approximations as introduced in (Colton, 1977) and extended in (Meurer and Kugi, 2009) does not show good convergence for time-varying kernels and is therefore only employed to investigate the existence of a solution. Thus, the presented solution will be based on a spatial discretisation of the kernel. However, in contrast to (Jadachowski et al., 2012) the Midpoint rule will be used which eventually leads to an iterative solution scheme that maintains the structural properties of the problem.

40 pt
0.556 in
14.1 mm

5.1 Integral Form

Introducing the normal form coordinates $\eta = \tilde{z} + \zeta$ and $\sigma = \tilde{z} - \zeta$ yields the dynamics

$$\partial_t \bar{k}(\eta,\sigma,t) = 4\alpha\partial_{\eta\sigma}\bar{k}(\eta,\sigma,t) + a\left(\tfrac{\eta-\sigma}{2},t\right)\bar{k}(\eta,\sigma,t) \tag{27a}$$

$$4\alpha\bar{k}(\eta,0,t) = \int_0^\eta a\left(\tfrac{r}{2},t\right)\,\mathrm{d}r - 4\bar{b}(0,t) \tag{27b}$$

$$\alpha\bar{k}(\eta,\eta,t) = \int_0^\eta \bar{b}\left(\tfrac{\eta+s}{2},t\right)\bar{k}(\eta,s,t)\,\mathrm{d}s - \bar{b}(\eta,t) \tag{27c}$$

of the transformed kernel $\bar{k}(\eta,\sigma,t) = \tilde{k}(\tilde{z},\zeta,t)$. Hence, formal integration of (27a) wrt. σ and η as well as substitution of (27b) (derived wrt. η) and (27c) yields

[1] Note, that to rigorously proof the invertability, the transformation has to be defined as a linear map on an appropriately chosen Banach space in order to make the underlying fixed point theory applicable. For lack of space, details are omitted within this contribution.

[2] As only variables of one phase occur in the kernel equations, the generic placeholder $\circ$ is dropped in favour of a more compact notation from now on.

$$\bar{k}(\eta,\sigma,t) = \frac{1}{4\alpha}\left\{\int_\sigma^\eta \left[a\left(\tfrac{r}{2},t\right) + \int_0^\sigma \left(\partial_t \bar{k}(r,s,t) - a\left(\tfrac{r-s}{2},t\right)\bar{k}(r,s,t)\right)\mathrm{d}s\right]\mathrm{d}r\right\} + \frac{1}{\alpha}\left(\int_0^\sigma \bar{b}\left(\tfrac{\sigma+s}{2},t\right)\bar{k}(\sigma,s,t)\,\mathrm{d}s - \bar{b}(\sigma,t)\right). \tag{28}$$

5.2 Existence

As already presented in (Colton, 1977) a solution for (28) by means of the method of successive approximations can be established by considering the series

$$\bar{k}(\eta,\sigma,t) = \sum_{n=0}^{\infty} \bar{K}^n(\eta,\sigma,t) \tag{29}$$

where the $\bar{K}^n(\eta,\sigma,t)$ are given by $\bar{K}^0(\eta,\sigma,t) = 0$,

$$\bar{K}^1(\eta,\sigma,t) = \int_\sigma^\eta a\left(\tfrac{r}{2},t\right)\mathrm{d}r - \frac{1}{\alpha}\bar{b}(\sigma,t) \tag{30a}$$

$$\bar{K}^n(\eta,\sigma,t) = \frac{1}{\alpha}\int_0^\sigma \bar{b}\left(\tfrac{\sigma+s}{2},t\right)\bar{K}^{n-1}(\sigma,s,t)\,\mathrm{d}s + \frac{1}{4\alpha}\int_\sigma^\eta\int_0^\sigma \left(\partial_t \bar{K}^{n-1}(r,s,t) - a\left(\tfrac{r-s}{2},t\right)\bar{K}^{n-1}(r,s,t)\right)\mathrm{d}s\,\mathrm{d}r \tag{30b}$$

Furthermore, Meurer and Kugi (2009) show that the convergence conditions on the series (29) depend on an upper bound for $\partial_t^l \bar{K}^n(\eta,\sigma,t)$ due to the repetitive differentiation in (30b). Although the detailed appearance may differ from the systems discussed in (Meurer and Kugi, 2009) or (Izadi et al., 2015), the terms that are to be examined are $a(\tilde{z},t)$ and $\bar{b}(\tilde{z},t)$.

Consider the term $a(\tilde{z},t)$, which is composed by the design parameter $\mu(\tilde{z},t)$ and the reaction coefficient $r(\tilde{z},t)$ of the error system. The latter coefficient, however, is mostly characterised by the reference interface velocity and acceleration which –as design parameters– are characterised by $\gamma_\mathrm{r}(t) \in \mathcal{G}_{\aleph\leq 2}(\mathbb{R}^+)$, (cf. 21a). Thus, by demanding $\mu(\tilde{z},t) \in \mathcal{K}_{\aleph\leq 2}(\Xi)$ with $\Xi = (0,\tilde{\Gamma}_\circ)\times\mathbb{R}^+$ it follows that $a(\tilde{z},t) \in \mathcal{K}_{\aleph\leq 2}(\Xi)$. Next, $\bar{b}(\tilde{z},t)$ from (21b) is given by the product of the reference temperature gradient $\partial_{\tilde{z}}\tilde{T}_{\circ,\mathrm{r}}(\tilde{z},t) \in \mathcal{K}_{\aleph\leq 2}(\Xi)$ and $\Psi_\circ^{-1}(\tilde{z},t)$. The inverse of the transformation (19) in turn is a simple composition of $\dot{\gamma}_\mathrm{r}(t)$ and the exponential function which does not affect the Gevrey order (Gevrey, 1918). Hence, $\bar{b}(\tilde{z},t)$ is from $\mathcal{K}_{\aleph\leq 2}(\Xi)$.

Summarising, the method employed in (Meurer and Kugi, 2009) can be adapted to this case to show existence for and uniqueness of the solution.

5.3 Approximation Scheme

For the spatial discretisation, values of the kernel are computed at selected grid points, given by $\bar{k}_{i,j}(t) = \bar{k}(i\Delta_\eta, j\Delta_\sigma, t)$ with the grid widths Δ_η and Δ_σ in η- and σ-direction, respectively. Due to the varying extent of the kernel domain, the computation grid is taken as the maximum extent for each respective phase, given by $\Delta\Gamma = \Gamma_\mathrm{l} - \Gamma_\mathrm{s}$. This yields the number of nodes $N_\eta = 2\Delta\Gamma/\Delta_\eta$ and $N_\sigma = \Delta\Gamma/\Delta_\sigma$ in each direction.

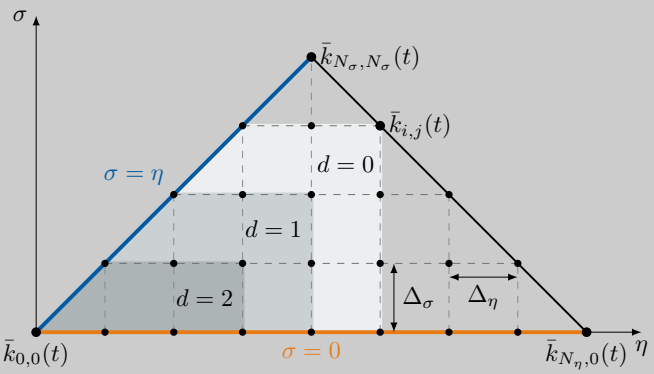

Fig. 2. Discretised kernel domain with selected kernel elements and required derivative orders for the computation of $k_{i,j}(t)$ (shaded).

Next, the uniform step width $\Delta = \Delta_\eta = \Delta_\sigma$, motivated by the similar dynamics in both directions, is chosen. Hence, approximating the integrals in (28) by lower sums yields the explicit computation scheme

$$\bar{k}_{i,j}(t) = \frac{\Delta^2}{4\alpha}\sum_{n=j}^{i-1}\sum_{m=0}^{j-1}\left(\partial_t\bar{k}_{n,m}(t) - a\left(\tfrac{n-m}{2}\Delta,t\right)\bar{k}_{n,m}(t)\right) + \frac{\Delta}{4\alpha}\sum_{n=j}^{i-1} a\left(\tfrac{n}{2}\Delta,t\right) - \frac{1}{\alpha}\bar{b}(j\Delta,t) + \frac{\Delta}{\alpha}\sum_{m=0}^{j-1}\bar{b}\left(\tfrac{j+m}{2}\Delta,t\right)\bar{k}_{j,m}(t) \tag{31}$$

for the interior where $0 < j < N_\sigma$ and $j < i < N_\eta - j$ while the boundary expressions are given by

$$\bar{k}_{i,0}(t) = \frac{\Delta}{4\alpha}\left(\sum_{m=0}^{i-1} a\left(\tfrac{m}{2}\Delta,t\right) - 4\bar{b}(0,t)\right) \tag{32}$$

$$\bar{k}_{j,j}(t) = \frac{1}{\alpha}\left(\Delta\sum_{n=0}^{j-1}\bar{b}\left(\tfrac{j+n}{2}\Delta,t\right)\bar{k}_{j,n}(t) - \bar{b}(j\Delta,t)\right) \tag{33}$$

for $0 \leq i \leq N_\eta$ and $0 \leq j \leq N_\sigma$, respectively. For the computation of an arbitrary kernel element $\bar{k}_{i,j}(t)$ via (31) the temporal derivatives of the neighbouring elements still pose a problem. However, all temporal derivatives of $\bar{k}_{i,j}(t)$ can be recursively substituted until only derivatives of $a(\tilde{z},t)$ and $\bar{b}(\tilde{z},t)$ remain. This gives the map

$$\bar{k}_{i,j}(t) = \Theta_{i,j}\left(a^{(0)},\ldots,a^{(j)},\bar{b}^{(0)},\ldots,\bar{b}^{(j)}\right) \tag{34}$$

which is further discussed in Appendix C.

Hence, given the structures of $a(\tilde{z},t)$ and $\bar{b}(\tilde{z},t)$, the complete kernel can be expressed as a function of the reference trajectory for the flat output $\boldsymbol{y}(t)$ of (7), its derivatives, and the design parameter $\mu(\tilde{z},t)$. Note that in (Jadachowski et al., 2012) this property is lost since an initial value problem has to be solved for the inner kernel elements, while the presented approach converges to the solution via successive approximations (29) for sufficiently small step sizes. However, the usage of the trapezoidal rule as in (Jadachowski et al., 2012) drastically reduces the approximation error for similar grid sizes due to the implicit nature of the resulting approximation scheme.

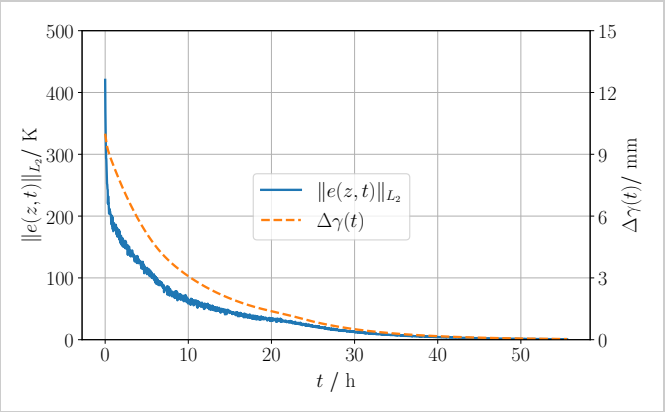

Fig. 3. Trajectories of the temperature errors L_2 norm (solid) and the interface deviation $\Delta\gamma(t)$ (dashed).

6. SIMULATION SETUP AND RESULTS

This section briefly presents simulation results for the two-phase case. The simulated process goal is the growth of a GaAs single crystal in a 400 mm furnace. As simulation model, a lumped, FE-based approximation with 41 nodes per phase has been used. For further details on the physical parameters of the simulation setup, please refer to (Ecklebe et al., 2019, Sec. 7).

In this case, the growth process shall start at an initial length of 200 mm and end at about 300 mm. To do so, $y_{\mathrm{r},2}(t)$ is chosen as a smooth transition (cf. (13)) between these values with the targeted solid phase gradient at the interface held constant at $y_{\mathrm{r},1}(t) = 17\,\mathrm{K\,m^{-1}}$ during the transition ($t < 25\,\mathrm{h}$). Thus, the recursion (9) from Section 3 yields the reference temperature trajectory $t \mapsto T_{\mathrm{r}}(\cdot, t)$ which in turn enables the computation of the kernels for the solid and liquid phases by means of (34). Herein, 81 discrete points and the parameters $\mu(\tilde{z}, t) = -1 \times 10^{-2}\,\mathrm{s^{-1}}$ as well as $\nu = 0\,\mathrm{m^{-1}}$ have been used in the target systems of both phases (cf. (22)). Finally, the control input is computed via (26).

For demonstration purposes, an initial error for the phase boundary of $\Delta\gamma(0) = 10\,\mathrm{mm}$ as well $\Delta\dot{\gamma}(0) = -3\,\mathrm{mm\,h^{-1}}$ for the growth velocity have been introduced. As shown in Figure 3, the controller ensures convergence for the error system $e(z,t)$ as well as the interface deviation $\Delta\gamma(t)$.

7. CONCLUSION AND OUTLOOK

In this contribution, a backstepping-based tracking control has been presented for a two-phase Stefan problem, occurring in the VGF process. By utilising both system inputs, this approach enables the tracking of arbitrary [3] reference trajectories. Although only a linear approximation of the error system is used, the results are promising. However, the stability proof of the modified target system for the two-phase case remains open. Moreover, for output feedback in practical applications, the proposed feedback has to be complemented by an appropriate observer. While two early-lumping observers are presented in (Ecklebe et al., 2019) by the authors for the TPSP and a late-lumping design is given in (Koga et al., 2019) for the OPSP, the treatment of the two-phase case with the backstepping method still remains open. These issues are currently under investigation and will be addressed in a more detailed article.

[3] The only hard restriction on the chosen references is given by the Gevrey order condition which is rather easy to satisfy.

REFERENCES

Cannon, J. R., 1984. The One-Dimensional Heat Equation. Vol. 23 of Encyclopedia of Mathematics and its Applications. Addison-Wesley.

Colton, D., 1977. The solution of initial-boundary value problems for parabolic equations by the method of integral operators. Journal of Differential Equations 26 (2), 181 – 190.

Crank, J., 1984. Free and Moving Boundary Problems (Oxford Science Publications). Oxford Science Publications. Oxford University Press.

Dunbar, W. B., Petit, N., Rouchon, P., Martin, P., 2003. Motion planning for a nonlinear Stefan problem. European Series in Applied and Industrial Mathematics (ESAIM): Control, Optimization and Calculus of Variations 9, 275–296.

Ecklebe, S., Woittennek, F., Winkler, J., Frank-Rotsch, C., Dropka, N., 2019. Towards model based control of the Vertical Gradient Freeze crystal growth process, available at `https://arxiv.org/abs/1908.02519`.

Gevrey, M., 1918. Sur la nature analytique des solutions des équations aux dérivées partielles. Premier mémoire. Annales scientifiques de l'École Normale Supérieure 35, 129–190.
URL `http://eudml.org/doc/81374`

Heuser, H., 1992. Funktionalanalysis Theorie und Anwendung, 3rd Edition. Teubner, Stuttgart.

Hinze, M., Pätzold, O., Ziegenbalg, S., 2009. Solidification of a GaAs melt—Optimal control of the phase interface. Journal of Crystal Growth 311 (8), 2501 – 2507.

Hopf, E., 1950. The partial differential equation $u_t + uu_x = \mu u_{xx}$. Communications on Pure and Applied Mathematics 3 (3), 201–230.

Izadi, M., Abdollahi, J., Dubljevic, S. S., 2015. PDE backstepping control of one-dimensional heat equation with time-varying domain. Automatica 54, 41 – 48.

Jadachowski, L., Meurer, T., Kugi, A., 2012. An efficient implementation of backstepping observers for time-varying parabolic pdes. IFAC Proceedings Volumes 45 (2), 798 – 803, 7th Vienna International Conference on Mathematical Modelling.

Jurisch, M., Börner, F., Bünger, T., Eichler, S., Flade, T., Kretzer, U., Köhler, A., Stenzenberger, J., Weinert, B., 2005. LEC- and VGF-growth of SI GaAs single crystals—recent developments and current issues. Journal of Crystal Growth 275 (1), 283 – 291, proceedings of the 14th International Conference on Crystal Growth and the 12th International Conference on Vapor Growth and Epitaxy.

Kang, S., Zabaras, N., 1995. Control of the freezing interface motion in two-dimensional solidification processes using the adjoint method. International Journal for Numerical Methods in Engineering 38 (1), 63–80.

Koga, S., Diagne, M., Krstic, M., Feb 2019. Control and State Estimation of the One-Phase Stefan Problem via Backstepping Design. IEEE Transactions on Automatic Control 64 (2), 510–525.

Koga, S., Krstic, M., May 2019. Single-Boundary Control of the Two-Phase Stefan System. arXiv e-prints, arXiv:1905.12735.

Maidi, A., Corriou, J.-P., 2016. Boundary Geometric Control of a Nonlinear Diffusion System with Time-Dependent Spatial Domain. Asian Journal of Control 18 (4), 1259–1268.

Meurer, T., Kugi, A., 2009. Tracking control for boundary controlled parabolic PDEs with varying parameters: Combining backstepping and differential flatness. Automatica 45 (5), 1182 – 1194.

Petrus, B., Bentsman, J., Thomas, B., 2012. Enthalpy-based feedback control algorithms for the Stefan problem. In: Proceedings of the IEEE Conference on Decision and Control. pp. 7037–7042.

Petrus, B., Bentsman, J., Thomas, B. G., 2010. Feedback control of the two-phase Stefan problem, with an application to the continuous casting of steel. In: 49th IEEE Conference on Decision and Control (CDC). pp. 1731–1736.

Petrus, B., Bentsman, J., Thomas, B. G., 2014. Application of Enthalpy-Based Feedback Control Methodology to the Two-Sided Stefan Problem. In: 2014 American Control Conference. pp. 1015–1020.

Rudolph, J., Winkler, J., Woittennek, F., 2003. Flatness based control of distributed parameter systems: Examples and computer exercises from various technological domains. Berichte aus der Steuerungs- und Regelungstechnik. Shaker Verlag, Aachen.

Rudolph, J., Winkler, J., Woittennek, F., 2004. Flatness based trajectory planning for two heat conduction problems in crystal growth technology. e-STA (Sciences et Technologies de l'Automatique) 1 (1).

Stefan, J., 1891. Über die Theorie der Eisbildung, insbesondere über die Eisbildung im Polarmeere. Annalen der Physikalischen Chemie, 269–286.

Appendix A. ERROR SYSTEM DYNAMICS

Taking the temporal derivative of (14a) and substituting (7a) for the original and reference temperature yields

$$\begin{aligned}\partial_t \tilde{e}_\circ(\tilde{z},t) &= \partial_t \tilde{T}_\circ(\tilde{z},t) - \partial_t \tilde{T}_{\circ,\mathrm{r}}(\tilde{z},t)\\ &= \alpha_\circ \partial_{\tilde{z}}^2 \tilde{T}_\circ(\tilde{z},t) + \dot{\gamma}(t)\partial_{\tilde{z}}\tilde{T}_\circ(\tilde{z},t)\\ &\quad - \alpha_\circ \partial_{\tilde{z}}^2 \tilde{T}_{\circ,\mathrm{r}}(\tilde{z},t) - \dot{\gamma}_\mathrm{r}(t)\partial_{\tilde{z}}\tilde{T}_{\circ,\mathrm{r}}(\tilde{z},t)\end{aligned}$$

which by substituting (14a), derived wrt. $\tilde{z}$ twice, becomes:

$$= \alpha_\circ \partial_{\tilde{z}}^2 \tilde{e}_\circ(\tilde{z},t) + \dot{\gamma}(t)\partial_{\tilde{z}}\tilde{T}_\circ(\tilde{z},t) - \dot{\gamma}_\mathrm{r}(t)\partial_{\tilde{z}}\tilde{T}_{\circ,\mathrm{r}}(\tilde{z},t).$$

Furthermore, replacing $\dot{\gamma}(t)$ and $\tilde{T}_\circ(\tilde{z},t)$ via (14a) and (14b), respectively, gives

$$\begin{aligned}\partial_t \tilde{e}_\circ(\tilde{z},t) &= \alpha_\circ \partial_{\tilde{z}}^2 \tilde{e}_\circ(\tilde{z},t) - \dot{\gamma}_\mathrm{r}(t)\partial_{\tilde{z}}\tilde{T}_{\circ,\mathrm{r}}(\tilde{z},t)\\ &\quad + \Big(\Delta\dot{\gamma}(t) + \dot{\gamma}_\mathrm{r}(t)\Big)\Big(\partial_{\tilde{z}}\tilde{e}_\circ(\tilde{z},t) + \partial_{\tilde{z}}\tilde{T}_{\circ,\mathrm{r}}(\tilde{z},t)\Big)\end{aligned}$$

and thus

$$\begin{aligned}\partial_t \tilde{e}_\circ(\tilde{z},t) &= \alpha_\circ \partial_{\tilde{z}}^2 \tilde{e}_\circ(\tilde{z},t) + \big(\Delta\dot{\gamma}(t)\partial_{\tilde{z}} + \dot{\gamma}_\mathrm{r}(t)\partial_{\tilde{z}}\big)\tilde{e}_\circ(\tilde{z},t)\\ &\quad + \Delta\dot{\gamma}(t)\partial_{\tilde{z}}\tilde{T}_{\circ,\mathrm{r}}(\tilde{z},t). \qquad \text{(A.1)}\end{aligned}$$

Finally, examining the boundaries yields

$$\tilde{e}_\circ(0,t) = \tilde{T}_\circ(0,t) - \tilde{T}_{\circ,\mathrm{r}}(0,t) = T_\mathrm{m} - T_\mathrm{m} = 0 \qquad \text{(A.2)}$$

$$\begin{aligned}\partial_{\tilde{z}}\tilde{e}_\circ\left(\tilde{\Gamma}_\circ,t\right) &= \partial_{\tilde{z}}\tilde{T}_\circ\left(\tilde{\Gamma}_\circ,t\right) - \partial_{\tilde{z}}\tilde{T}_{\circ,\mathrm{r}}\left(\tilde{\Gamma}_\circ,t\right)\\ &= \frac{\delta_\circ}{\lambda_\circ}u_\circ(t) - \partial_{\tilde{z}}\tilde{T}_{\circ,\mathrm{r}}(\tilde{\Gamma},t) = \tilde{u}_\circ(t). \qquad \text{(A.3)}\end{aligned}$$

Appendix B. KERNEL EQUATIONS

To derive the mandatory conditions on the transformation kernel from (23), the derivatives of (23) are taken wrt. t and $\tilde{z}$. Next, they are substituted in (22a) to express the target system dynamics in terms of the original error $\tilde{e}_\circ(\tilde{z},t)$. Furthermore, (15) is substituted and integration by parts is performed to shift the spatial operators onto $\tilde{k}(\tilde{z},\zeta,t)$. Finally, since the resulting equation has to hold for all $\tilde{e}_\circ(\tilde{z},t)$, one arrives at the kernel equations

$$\begin{aligned}\partial_t k_\circ(\tilde{z},\zeta,t) &= \alpha_\circ\left(\partial_{\tilde{z}}^2 k_\circ(\tilde{z},\zeta,t) - \partial_\zeta^2 k_\circ(\tilde{z},\zeta,t)\right)\\ &\quad + a_\circ(\zeta,t)k_\circ(\tilde{z},\zeta,t) \qquad \text{(B.1a)}\\ a_{\circ(\tilde{z},t)} &= 2\alpha_\circ \tfrac{\mathrm{d}}{\mathrm{d}\tilde{z}}k_\circ(\tilde{z},\tilde{z},t) \qquad \text{(B.1b)}\\ \alpha_\circ k_\circ(\tilde{z},0,t) &= \int_0^{\tilde{z}} \bar{b}_\circ(\zeta,t)k_\circ(\tilde{z},\zeta,t)\,\mathrm{d}\zeta - \bar{b}_\circ(\tilde{z},t) \qquad \text{(B.1c)}\\ 0 &= \int_0^{\tilde{z}} \bar{c}_\circ(\zeta,t)k_\circ(\tilde{z},\zeta,t)\,\mathrm{d}\zeta - \bar{c}_\circ(\tilde{z},t). \qquad \text{(B.1d)}\end{aligned}$$

Thus, integration of (B.1b) yields

$$k_\circ(\tilde{z},\tilde{z},t) = \frac{1}{2\alpha_\circ}\int_0^{\tilde{z}} a_\circ(\zeta,t)\,\mathrm{d}\zeta + k_\circ(0,0,t)$$

where $k_\circ(0,0,t) = -b_\circ(\tilde{z},t)/\alpha_\circ$ from (B.1c) at $\tilde{z}=0$.

Appendix C. DERIVATIVE ORDERS

To analyse the required derivative orders for the computation of an arbitrary kernel element $\bar{k}_{i,j}(t)$ the l-th derivative of (31)

$$\begin{aligned}\partial_t^l \bar{k}_{i,j}(t) &= \frac{\Delta^2}{4\alpha}\sum_{n=j}^{i-1}\sum_{m=0}^{j-1}\Bigg(\partial_t^{(l+1)}\bar{k}_{n,m}(t)\\ &\quad - \sum_{d=0}^{l}\binom{l}{d}\partial_t^{(l)}a\left(\tfrac{n-m}{2}\Delta,t\right)\partial_t^{(l-d)}\bar{k}_{n,m}(t)\Bigg)\\ &\quad + \frac{\Delta}{\alpha}\sum_{m=0}^{j-1}\sum_{d=0}^{l}\binom{l}{d}\partial_t^{(l)}\bar{b}\left(\tfrac{j+m}{2}\Delta,t\right)\partial_t^{(l-d)}\bar{k}_{j,m}(t)\\ &\quad - \frac{1}{\alpha}\partial_t^l\bar{b}\left(j\Delta,t\right) + \frac{\Delta}{4\alpha}\sum_{n=j}^{i-1}\partial_t^l a\left(\tfrac{n}{2}\Delta,t\right) \qquad \text{(C.1)}\end{aligned}$$

is examined. As it can be seen, for every derivative in (31) that is to be eliminated, derivatives of the kernel elements below and left of one order higher, as well as derivatives of the provided functions $a(\tilde{z},t)$ and $\bar{b}(\tilde{z},t)$ with the same order are introduced (cf. shaded areas in Figure 2). Therefore, the computation of $\bar{k}_{i,j}(t)$ demands a derivative order of $\min\{i,j\} = j$ for these functions. Hence, for the computation of the complete kernel, $d_{\max} = N_\sigma - 1$ derivatives are required as the kernel element $\bar{k}_{N_\sigma,N_\sigma}(t)$ is already given by (33).